Atmos. Meas. Tech. Discuss., 8, 8113–8156, 2015
www.atmos-meas-tech-discuss.net/8/8113/2015/
doi:10.5194/amtd-8-8113-2015

Atmospheric Measurement Techniques Discussions

A dual, single detector relaxed eddy accumulation system for long-term measurement of mercury flux

S. Osterwalder[1], J. Fritsche[1], M. B. Nilsson[2], C. Alewell[1], J. Sommar[3], G. Jocher[2], M. Schmutz[1], J. Rinne[4,5], and K. Bishop[6,7]

[1]Department of Environmental Sciences, University of Basel, Basel, Switzerland
[2]Department of Forest Ecology and Management, Swedish University of Agricultural Sciences, Umeå, Sweden
[3]State Key Laboratory of Environmental Geochemistry, Chinese Academy of Sciences, Guiyang, China
[4]Department of Geosciences and Geography, University of Helsinki, Helsinki, Finland
[5]Finnish Meteorological Institute, Helsinki, Finland
[6]Department of Aquatic Sciences and Assessment, Swedish University of Agricultural Sciences, Uppsala, Sweden
[7]Department of Earth Sciences, University of Uppsala, Uppsala, Sweden

Received: 5 June 2015 – Accepted: 7 July 2015 – Published: 5 August 2015

Correspondence to: S. Osterwalder (stefan.osterwalder@unibas.ch)

Published by Copernicus Publications on behalf of the European Geosciences Union.

AMTD
8, 8113–8156, 2015

Abstract

The fate of anthropogenic emissions of mercury (Hg) to the atmosphere is influenced by the exchange of elemental Hg with the earth surface. This exchange which holds the key to a better understanding of Hg cycling from local to global scales has been difficult to quantify. To advance and facilitate research about land–atmosphere Hg interactions, we developed a dual-intake, single analyzer Relaxed Eddy Accumulation (REA) system. REA is an established technique for measuring turbulent fluxes of trace gases and aerosol particles in the atmospheric surface layer. Accurate determination of gaseous elemental mercury (GEM) fluxes has proven difficult to technical challenges presented by extremely small concentration differences (typically $< 0.5\,\mathrm{ng\,m^{-3}}$) between updrafts and downdrafts. To address this we present an advanced REA design that uses two inlets and two pair of gold cartridges for semi-continuous monitoring of GEM fluxes. They are then analyzed sequentially on the same detector while another pair of gold cartridges takes over the sample collection. We also added a reference gas module for repeated quality-control measurements. To demonstrate the system performance, we present results from field campaigns in two contrasting environments: an urban setting with a heterogeneous fetch and a boreal mire during snow-melt. The observed emission rates were 15 and $3\,\mathrm{ng\,m^{-2}\,h^{-1}}$. We claim that this dual-inlet, single detector approach is a significant development of the REA system for ultra-trace gases and can help to advance our understanding of long-term land–atmosphere GEM exchange.

1 Introduction

The UN's legally binding Minimata Convention was agreed upon by 147 nations in 2013 and aims to protect human health and welfare by reducing anthropogenic release of mercury (Hg) into the environment (UNEP, 2013a). Current anthropogenic sources, mainly from fossil fuel combustion, mining, waste incineration and industrial processes, are responsible for about 30 % of annual Hg emissions to the atmosphere. 10 % come

AMTD
8, 8113–8156, 2015

from natural geological sources and the remaining 60 % from re-emission of previously deposited Hg (UNEP, 2013b). As a result, long-range atmospheric transport of gaseous elemental mercury (GEM or Hg^0) has led to Hg deposition and accumulation in soils and water bodies well in excess of natural levels even in remote areas, far away from anthropogenic pollution sources (Slemr et al., 2003; Grigal, 2002).

Quantification of Hg emission and deposition is needed to reduce the large gaps that exist in the global Hg mass balance estimates (Mason and Sheu, 2002) and as a basis of legislation targeting the control of Hg emissions (Lindberg et al., 2007). Gustin et al. (2008) suggest that today a substantial amount of Hg deposited on soils is reemitted back to the atmosphere. Over an annual cycle the deposition is largely compensated by re-emission resulting in a net flux close to zero.

The state-of-the-art in field techniques to quantify Hg flux from terrestrial surfaces has been summarized in review papers (Gustin et al., 2005, 2008, 2011; Sommar et al., 2013b). They conclude that environmental, physicochemical and meteorological factors as well as surface characteristics determine the accuracy and precision of GEM measurements. Fluxes are commonly determined using dynamic flux chambers (DFCs) or micrometeorological techniques (Relaxed Eddy Accumulation [REA], modified Bowen-ratio [MBR] or the aerodynamic gradient [AER] method). DFCs are the most widely used technique to measure in situ GEM fluxes since they are easy to handle and inexpensive. But DFCs alter the environment of the area being studied by affecting atmospheric turbulence, temperature and humidity. Their application is therefore restricted to short term measurements (Cobos et al., 2002) and studies comparing the relative differences between sites only, e.g. control and treatment experiments (Fritsche et al., 2014).

A major advantage of micrometeorological techniques is that they are conducted under conditions with minimal disturbance. As they can be applied continuously, they provide flux data valuable for deducing regulating mechanisms and seasonal patterns. Micrometeorological techniques are also able to cover a much larger area than DFC techniques, although this larger "footprint" should be relatively flat and homogeneous.

AMTD
8, 8113–8156, 2015

Several studies report results from GEM land–atmosphere exchange measurements over a variety of landscapes using AER and MBR techniques (e.g. Meyers et al., 1996; Lindberg and Meyers, 2001; Kim et al., 1995; Gustin et al., 2000; Converse et al., 2010; Fritsche et al., 2008b). Fritsche et al. (2008a) concluded that micrometeorological techniques are appropriate to estimate Hg exchange rates but often suffered from large uncertainties due to extremely low concentration gradients over background soils ($< 0.1\,\mu g\,Hg\,g^{-1}$). Eddy Covariance (EC) has the potential to detect high frequency GEM concentration fluctuations and might improve flux estimates considerably (Bauer et al., 2002; Faïn et al., 2010). Pierce et al. (2015) conducted the first successful EC flux measurements of GEM over Hg-enriched soils measuring GEM concentrations at high frequency (25 Hz). However, on background soils measured fluxes were below the detection limit.

To overcome the need for fast-response sensors, a modification of the EC technique was proposed by Desjardin et al. (1972, 1977) where fast-response sampling valves are combined with slow analysis techniques on the assumption that the turbulent covariance flux can be averaged separately for positive and negative vertical wind velocities. The technical breakthrough for REA was achieved by Businger and Oncley (1990), simulating the method with vertical wind, temperature and humidity time series in the surface layer. The main advantage of REA over other micro-meteorological methods is that REA requires sampling at only one height. Reactive substances can be lost by chemical reaction between two sampling heights (Foken, 2006; Fritsche et al., 2008a; Olofsson et al., 2005a), and sensors at two heights also have different footprints. REA eliminates these drawbacks (Bash and Miller, 2008).

The REA method has been widely used since 1990 to investigate fluxes of different trace gases and aerosols (e.g. Brut et al., 2004; Gaman et al., 2004; Olofsson et al., 2005a; Haapanala et al., 2006; Arnts et al., 2013). This includes a few applications on land–atmosphere GEM exchange over soils (Cobos et al., 2002; Olofsson et al., 2005b; Sommar et al., 2013a; Zhu et al., 2015a) and forest canopies (Bash and Miller, 2007, 2008, 2009). Additionally, reactive gaseous Hg fluxes have been measured over

AMTD
8, 8113–8156, 2015

snow surfaces in the Arctic (Skov et al., 2006). Besides valuable data of net exchange rates of GEM over different environments, the studies have also identified potential for refinement in the technical implementation of REA. The dual detector system presented by Olofsson et al. (2005b) was criticized since it suffered from inherent variability and drift of sensitivity between the two Hg detectors (Sommar et al., 2013a). Sommar et al. (2013a) modified the systems employed by Cobos et al. (2002) and Bash and Miller (2008) to create a single-inlet REA system. However, their system lacks the capability to accumulate samples from the up- and downdraft channels synchronously. The application of sequential measurement of the channels impairs the accuracy with which fluxes can be gauged when the concentration of ambient GEM varies on the scale of the sampling period (Zhu et al., 2015b).

Even though there has been steady improvement in REA systems for measuring Hg fluxes, the financial and technical challanges to accurately measure the extremely low concentration differences (sub-ppt range) in up- and downdrafts have limited the number of studies (Foken, 2006). Thus, there remains a demand for a system especially designed to continuously monitor background GEM fluxes with minimum maintenance requirements.

To address these needs we designed a fully automated dual-inlet REA system with a single Hg detector which is able to semi-continuously measure GEM fluxes over a homogenous terrestrial landscape. We intended to improve upon earlier REA systems with two features: (1) continuous, simultaneous sampling of Hg in up- and downdrafts by using two pairs of Hg-cartridges, and (2) regular sampling of a GEM standard as well as dry, Hg-free air to monitor instrument sensitivity.

To test the systems performance and its applicability we deployed it in two contrasting environments during campaigns of several weeks. At the first site in Switzerland, GEM fluxes were measured 20 m above the roof of a building, 38 m a.g.l. in an urban environment. Later on the system was installed 1.8 m above a boreal mire called Degerö in northern Sweden during snowmelt.

AMTD
8, 8113–8156, 2015

This paper includes a description of the novelties in the REA design and presents a time series of GEM flux measurements from each of the deployments with contrasting atmospheric conditions and site characteristics. To analyze the system performance we compared source-sink characteristics using footprint models and analyzed turbulence regimes to determine possible flux attenuation. We briefly discuss several instrumental factors which might affect the accuracy of the flux measurements: bias in vertical wind measurements, control and response time of the REA sampling valves, measurement precision of the sample volumes, as well as the performance of analytical schemes and calibration procedures. Furthermore we describe the evaluation of the β constant, the method detection limit and rejection criteria for flux measurements based on the REA validation procedure.

2 Materials and methods

2.1 Methodology

In REA systems, fast-response switching solenoid valves are controlled by the vertical wind velocity (w) signal of a 3-D Sonic Anemometer enabling sampling and separation of air into upward and downward moving air parcels (Businger and Oncley, 1990). GEM carried in the "updrafts" and "downdrafts" is thereby collected in separate reservoirs. The flux [ng m^{-2} h^{-1}] is calculated from the GEM concentration difference [ng m^{-3}] in updraft ($\overline{C_u}$) and downdraft ($\overline{C_d}$) air, multiplied by σ_w [m s^{-1}], the standard deviation of vertical wind velocity.

$$F_{GEM} = \beta \sigma_w (\overline{C_u} - \overline{C_d}) \quad (1)$$

β is the unitless flux proportionality coefficient and depends on the wind velocity deadband (see Sect. 3.1.2) that is implemented to increase the concentration difference. β values typically range between 0.4 and 0.6. Deadband widths [m s^{-1}] used in recent REA measurement studies range from 1/3 to 0.6 times σ_w (Grönholm et al., 2008). In

AMTD
8, 8113–8156, 2015

the present study a fixed deadband was used during the campaign in Basel and a dynamic deadband at Degerö. Applying a fixed deadband makes β dependent on atmospheric conditions (Milne et al., 1999, 2001) and increased deadband widths leading to lower β values (Ammann, 1999). A dynamic deadband is applied more often (cf. Gaman et al., 2004; Olofsson et al., 2005b; Haapanala et al., 2006; Ren et al., 2011) and enables the use of a constant β (Grönholm et al., 2008).

To compute β in Eq. (2), air temperature has to be sampled by an EC system at the same intervals used for the "up" and "down" GEM sampling system. β is determined from these "up" and "down" averages of temperature (θ_u and θ_d), σ_w and the measured EC sensible heat flux ($\overline{w'\theta'}$), calculated separately for each 30 min period.

$$\beta = \frac{(\overline{w'\theta'})}{\sigma_w(\overline{\theta_u} - \overline{\theta_d})} \tag{2}$$

In our application a recursive high-pass filter was implemented to reduce low-frequency bias in turbulent time series of the vertical wind velocity (McMillen, 1988; Richardson et al., 2012):

$$\chi_i = \alpha\chi_{i-1} + (1-\alpha)\chi \tag{3}$$

where χ_i is the filtered value, χ_{i-1} was the running mean from the previous time step, and χ the current, instantaneous value (Meyers et al., 2006).

$$\alpha = e^{-\frac{\Delta t}{\tau}} \tag{4}$$

The constant α results from the sampling interval of 10 Hz (Δt) and the time constant (τ) which was set to 1000 s (Eq. 4).

2.2 GEM sampling system

At both sites the REA system was connected to existing EC systems that have been measuring latent heat flux and CO_2 exchange at 30 min intervals (Lietzke and Vogt,

AMTD
8, 8113–8156, 2015

2013; Sagerfors et al., 2008) for many years. A suite of meteorological parameters is recorded as well: solar radiation, temperature, humidity, rainfall, snow depth and surface layer stability parameters. Figure 1 shows the REA-system units major components (see Table S1 in the Supplement for components used).

Sampling of the vertical wind velocity was done using a fast-response (10 Hz) 3-D Sonic anemometer (A1, A2). A laptop PC controlled the REA system using LabVIEW (National Instruments Corp., USA) which (B) filtered the vertical wind velocity signal and determined the switching intervals of the three fast-response valves (C). These separated the air into updraft (V1), downdraft (V2) and deadband (V3) channels. The valves are installed 0.2 m downstream of the sampling inlets. The inlets of the 1/4″-Teflon sampling lines (D) were mounted near the anemometer head about 15 cm below the midpoint of the ultrasound paths. The sampling lines were insulated to avoid condensation. 0.2 µm PTFE filters (E, F) were installed after the inlets and before the Teflon valves, V4 and V5 (G). The resistance through the sampling lines was checked to be equal using thermal mass flow meters (Vögtlin Instruments AG, Switzerland). Conditionally sampled GEM is subsequently accumulated on the gold cartridges. Heating wires around the cartridges were kept at 50 °C during the sampling phase and heated to 500 °C during the desorption process (see Sect. 2.3). Downstream, a pressure sensor (H) operating at 10 Hz was installed to monitor pressure fluctuations. A high-precision thermal mass flow controller (MFC) (I) with a response time of 50 ms was used to regulate the air volume drawn over the gold cartridges. To dampen sampling flow disturbances a reservoir of 200 mL was installed between the pump and the MFC. Air was drawn through the three lines by a rotary vane pump (J) at a rate of 1 L min^{-1} (Basel) and 1.5 L min^{-1} (Degerö), respectively. Three temperature-controlled, weatherproof boxes (K) contained the Hg permeation source (L) and Hg detector (M), the gold cartridge unit and the control system as well as a filter unit to produce dry, Hg-free air. Remote control of the system allowed online checks of the data and detection of instrumental failures.

AMTD
8, 8113–8156, 2015

2.3 GEM analysis

Air sampling and GEM analysis was performed in parallel in 30 min intervals (Fig. 2). GEM in air samples and injections from the Hg permeation source and zero-air unit were quantified using Cold Vapor Atomic Fluorescence Spectrophotometry (CVAFS) (M). The temperature controlled Hg permeation source (operated at 46 °C in Basel and 35 °C at Degerö) provided concentrations similar to ambient air levels (1.2–4 ng m^{-3}). Dry, Hg-free air was generated using an air compressor (N) with air dryer (O) and an activated carbon filter (P). Additional gold mercury scrubbers were installed at the outlet of the zero-air unit.

Figure 2 illustrates the sampling and analysis sequence. Upon startup cartridges C2 and C4 are in the air sampling mode, while GEM previously collected on C1 and C3 is analyzed. During the first 5 min GEM of the idle cartridges is desorbed by heating the cartridges to 500 °C in a stream (80 mL min^{-1}) of high purity Argon (Ar) carrier gas (Q). The cartridge analysis procedure for individual samples included five steps: Ar-flushing (20 s), recording baseline (10 s), cartridge heating (28 s), peak delay (30 s) and cooling of the cartridges (60 s). After up- and downdraft air samples had been analyzed (Aa), the cartridges were loaded for 5 min each with either GEM reference air (ref) or dry, Hg-free air (clean). The air samples were analyzed alternately every hour. The flow rate of dry, Hg-free air (carrier gas) through the permeation source was set to 600 mL min^{-1} using a MFC. The reference gas was pre-mixed with 100 mL min^{-1} dry, Hg-free air before being supplied to the cartridges. Dry, Hg-free air was delivered at a flow rate of 1500 mL min^{-1} regulated by another MFC.

The cartridges loaded with ref/clean air were analyzed (Ab phase in Fig. 2) following the same procedure as the air samples. The average and standard deviation of the Hg detector baseline [mV] were calculated for periods of three seconds before and after the Hg peak. The baseline below the peak was interpolated and subtracted from the peak.

AMTD
8, 8113–8156, 2015

The peak areas were logged together with 30 min averages of the sampled air volume, opening times and number of switching operations of the fast-response valves. Air temperatures within the weatherproof boxes, Hg detector lamp- and UV sensor voltages as well as pressure sensor data were also recorded.

2.4 QA/QC

2.4.1 Calibration of Hg detector

The REA system was calibrated after the field campaigns using a temperature-controlled Hg vapor calibration unit (R) together with a digital syringe (S). Different concentrations of saturated GEM vapor were injected into the Hg-free air stream provided by a Hg zero air generator (T)(Table S1). During calibration a simulated wind signal was used to supply both lines with an equal amount of air. Calibration factors were gained by linear regression between the injected quantity of GEM and observed peak areas.

2.4.2 Monitoring of GEM recovery

Repeated injections from the Hg permeation source and dry, Hg-free air (Fig. 2) was performed to observe possible contamination, passivation or drift of the cartridges, as well as to check for temperature sensitivity in the Hg detector. Before and after a measurement campaign the system was checked for leaks by measuring dry, Hg-free air from the Hg zero air generator and by constricting the sampling lines temporarily to check for pressure decrease within the lines. PTFE parts and tubing were cleaned with 5 % nitric acid according to a standard operating procedure (adapted from Keeler and Landis, 1994).

AMTD
8, 8113–8156, 2015

2.4.3 Bias of sampling lines

To assess potential systematic bias between up- and downdraft sampling lines, GEM reference air from the permeation source was supplied to both lines. During four days in Basel and two days at Degerö, the REA-system dynamically sampled reference air using 2 s-simulated wind signal to acquire identical up- and downdraft samples with respect to volume and GEM concentration. Accordingly, concentration bias between the REA sampling lines was corrected for in the GEM flux calculation.

2.5 Data processing

The analyzed air samples (Aa) for each cartridge were corrected for temperature sensitivity of the Hg detector using the analyzed GEM reference air (Ab_r) according to:

$$A_{corr} = Aa \cdot \frac{\overline{Ab_r}}{Ab_r} \quad (5)$$

GEM concentrations ($\overline{C_{GEM}}$) in up- and downwind air were computed by applying intercept (b) and slopes (s) calculated from the manual calibration procedure (Sect. 2.4.1) and the air volumes (V) drawn over the cartridges:

$$\overline{C_{GEM}} = \frac{A_{corr} - b}{s} \cdot \frac{1}{V} \quad (6)$$

GEM concentration differences were corrected for the bias between the two sampling lines (Sect. 2.4.3). Finally, the GEM flux was derived following Eq. (1). As the sampled air was not dried before being measured with a MFC calibrated for dry air, GEM fluxes calculated by Eq. (1) were corrected for variations in the water vapor content of the air following Lee (2000):

$$F_{Hg_{corr}} = (1 + 1.85\chi_s)F_{Hg} + 1.85\frac{\overline{\rho}_{GEM}}{\overline{\rho}_a}LE_m, \quad (7)$$

AMTD
8, 8113–8156, 2015

where $F_{Hg_{corr}}$ is the corrected and F_{Hg} the uncorrected GEM flux [ng m^{-2} h^{-1}] while χ_s is the water vapor mixing ratio [kg kg^{-1}]. LE_m is the water vapor flux [ng m^{-2} h^{-1}], and the ratio of mean GEM density to mean air density must be determined from the data for each measurement interval.

Criteria to identify conditions under which REA is not valid have been determined in Sect. 3.1.4. Among them an integral turbulent characteristics test was applied to identify the development of turbulent conditions (Eq. 8) including σ_w, friction velocity (u_*), measuring height (z) and Obukhov length (L). Therein, the dependent integral turbulence characteristic for vertical wind velocity (σ_w/u_*) equates with a model dependent on stability (z/L) (Panofsky and Dutton, 1984; Foken and Wichura, 1996; Foken, 2006). A factor 2 deviation from the model was used as the threshold to reject periods of insufficient turbulence (Fig. S2 in the Supplement):

$$\frac{\sigma_w}{u_*} = 1.3 \cdot \left(1 - 2 \cdot \frac{z}{L}\right)^{\frac{1}{3}}. \quad (8)$$

The effect of a potentially dampened GEM flux due to the delay between momentum measurements and corresponding conditional sampling has been derived by interpretation of turbulence spectra for both sites dependent on instrumental properties (lateral sensor separation), measuring height, wind speed and stability conditions (Sect. 3.3). The applied high-pass filter (Eqs. 3 and 4) amplifies the attenuation by reducing random or systematic noise in the flux estimates caused by low-frequency bias in the turbulent time series. High frequency attenuation might be caused by an electronic delay of the valve switching and sensor separation (Foken et al., 2012).

To predict the size of REA flux source areas during the campaigns the footprint model of Kormann and Meixner (2001) was applied in Basel and a Lagrangian stochastic forward model following Rannik et al. (2003) at Degerö. The actual source area was estimated for each half-hour period based on wind direction, wind speed, stability, surface roughness and sensor height.

AMTD
8, 8113–8156, 2015

2.6 Site descriptions

The climate in the city of Basel, Switzerland (47.56° N, 7.58° E; 264 m a.s.l.) is temperate with a mean annual temperature of +9.8 °C and 776 mm precipitation (MeteoSchweiz, 2014). The REA system was deployed on the flat roof of the University of Basel's Meteorology, Climatology and Remote Sensing Laboratory (MCR) 20 m above the ground. The REA sampling inlets were mounted on the top of the permanently installed tower at 38 m a.g.l. The average building height around the tower is 17 m and the 90 % cumulative footprint mirrors dominant wind directions, which are W to NW (240–340°) and ESE (100–140°). Results from this site reflect the situation within the urban inertial sublayer (Lietzke and Vogt, 2013).

The second campaign was conducted at an Integrated Carbon Observatory System (ICOS) site in the center of a boreal mire in Sweden (64.18° N, 19.55° E; 270 m a.s.l.) during snowmelt. The mixed acid mire system covers 6.5 km^2 and is located in the Kulbäcksliden Research Park of the Svartberget Long-Term Experimental Research (LTER) facility near the town of Vindeln, county of Västerbotten, Sweden. The site is part of the Swedish research infra-structure (funded by the Swedish Research Council). The snow cover normally reaches a depth up to 0.6 m and lasts for 6 months on average (Sagerfors et al., 2008). The average total Hg concentrations (THg) in the upper 40 cm of the mire soil are 57.3±6.0 ng g^{-1} (±SD) dry matter, which is a typical value for soils in northern Sweden (Åkerblom et al., 2013; Shanley and Bishop, 2012). The climate of the site is defined as humid cold temperate with mean annual precipitation and temperature of 523 mm and +1.2 °C, respectively (Alexandersson et al., 1991). A measurement height of 1.8 m above the mire surface was maintained by gradually decreasing of the instrumentation boom to account for snowmelt. Dominant wind direction during summer is NE and SE during winter. For a more detailed site description see Granberg et al. (2001) or Peichl et al. (2013).

AMTD
8, 8113–8156, 2015

3 Results and discussion

3.1 REA performance

3.1.1 Sampling accuracy

Generally REA systems with two separate inlets for up- and downdraft are less prone to measurement uncertainty due to unsynchronized conditional sampling (Baker et al., 1992) and high frequency concentration fluctuations in the tube flow (Moravek et al., 2013). Zhu et al. (2015b) found that the largest source of uncertainty in their single-inlet Hg-REA system was the asynchronous sampling. Accurate simultaneous sampling of Hg concentration using a two-inlet design is the major technical improvement of our system compared to most Hg-REA systems used to date, as summarized in Sommar et al. (2013a). But even though the dual-inlet avoids a major source of error, there are a number of other aspects of a REA-Hg system that need to work as well as possible to measure land–atmosphere Hg fluxes. One of these is the determination of the β value, which includes Sonic anemometer temperature and sensible heat flux measurements (Sect. 3.1.2). It is estimated to introduce an uncertainty similar to Zhu et al. (2015b) of approximately 10 %. Uncertainty due to flux dampening of sampled low and high frequency concentration fluctuations is small and just relevant during specific stability and wind speed conditions depending on measurement height and quality of turbulence (Sect. 3.3). There are several other sources of error in the measurements such as the (i) the possible bias in vertical wind velocity measurements, (ii) the precision of the switching of the fast-response valves, (iii) the sampled air volume, (iv) the peak integration and (v) the field calibration procedure (cf. Zhu et al., 2015b).

i. Vertical wind velocity is used for instantaneous valve control. Ammann (1999) ascribed the main error here to be the possibility for misalignment between the wind field and the sensor head due to a tilted sensor setup or wind distortion around the sensor. However, the application of a high-pass filter combined with

AMTD
8, 8113–8156, 2015

a deadband was able to alleviate averaged vertical wind velocity bias from the wind signal.

ii. It is important to limit the electronic delay to switch the fast-response valves caused by the digital measurements system and signal processing. The effective response time to actuate the fast-response valves was determined to 18 ms for the opening and 8 ms for the closing. The change of the sign of the vertical wind velocity and the switching of the fast-response valves allowed a maximal resolution between updraft and downdraft samples of 5 Hz.

iii. A major challenge in applying a system with two inlet tubes and no dry Hg-free air addition at the inlets (as applied by Sommar et al., 2013a) is to control flow pressure that builds up within the sampling lines. Flow surges are dependent on the time the fast-response valves remain closed. Pressure variations were dampened by a reservoir of 200 mL volume between the pump and mass flow controller (Fig. 1). The resistance within the lines was initially checked to be equal to minimize pressure anomalies between the three flow paths. A simulated wind signal with fast-response valve opening times of 2 s for the up- and downdraft and 1 s for the deadband was applied and revealed maximal pressure fluctuations of 35 mbar. The vast majority of the 30 min measurements in Basel and Degerö showed higher switching rates which are generally associated with lower pressure fluctuations. At Basel and Degerö the sampled volumes averaged 30 ± 0.09 and 45 ± 0.01 L, respectively. Measurements were discarded if the volume deviated more than 2.5 % from the flow setting value of the mass flow controller (cf. Sect. 3.1.4).

iv. An analysis of the detector peaks indicated that the signal for ambient and GEM reference air samples were statistically different from blank measurements (99 % confidence) (Fig. 3). To retrace possible irregularities in the Hg detector baseline peaks the high resolution voltage data were logged.

AMTD
8, 8113–8156, 2015

v. The manual calibration procedure revealed a strong linear relationship between peak areas and syringe injected GEM reference air for the cartridge-pairs (Fig. S1). The automated injection of GEM reference air provided a two hourly QC-measure to monitor any bias caused by the temperature sensitivity of the Hg detector. The ambient air temperature surrounding the Hg detector showed a strong linear relationship with the GEM reference air measurements for up- and downdraft in Basel and a less pronounced dependence at Degerö (Fig. 4). The uncertainty of concentration measurements for our REA system is basically introduced by sampling-line bias, wherefrom the method detection limit is derived (Sects. 2.4.3 and 3.1.3).

3.1.2 β factor evaluation

In this study, β is derived from EC time series of temperature and vertical wind speed at both sites (Eq. 2) during methodologically favorable conditions (cf. Sect. 3.1.4) with respect to turbulence for every 30 min GEM flux measurement averaging period. Due to considerable scatter in β especially during periods when sensible heat flux diminished to near zero, data were omitted for kinematic heat flux $\pm 0.01\,\mathrm{K\,m\,s^{-1}}$ (Ammann and Meixner, 2002; Sommar et al., 2013a). In accordance with Hensen et al. (2009) only β factors in the range of 0.1–1 were used. During the first study in Basel a fixed deadband of $|w| < 0.2\,\mathrm{m\,s^{-1}}$ was applied. This was done to restrict the analysis to periods when the discrimination between updraft and downdraft was large enough to allow for accurate estimation and to prolong the opening times of the fast-response valves. At Degerö a dynamic deadband approach with a sampling threshold $\pm 0.5\sigma_w$ was used. Data analysis revealed that the effect of surface layer stability or u_* on β calculation was negligible. The median ± mad (median absolute deviation) of observed β values in Basel and Degerö was 0.49 ± 0.21 ($n = 391$) and 0.45 ± 0.20 ($n = 342$), respectively. Median β values observed at Basel and Degerö concurred with literature in the range of 0.4–0.6 as listed in Grönholm et al. (2008); Bash and Miller (2009); Arnts et al. (2013); Sommar et al. (2013a).

AMTD
8, 8113–8156, 2015

The Basel measurements resulted in broad non-Gaussian frequency distributions for the fraction of time when air was sampled into up- and down reservoirs. The average cumulated opening times for the 30 min sampling periods for the up- and downdrafts were 9.6 and 9.8 min respectively, which results in maxima in up/down/deadband sampling fractions of about 32 %/33 %/35 %. Periods of less developed turbulence caused the fast-response valves to switch less often and increased the opening times of the deadband. The corresponding confined frequency distributions observed at Degerö were 28 %/27 %/45 % and show significantly lower variation than for the Basel measurements.

3.1.3 Detection limit

The instrument detection limit of the Hg detector was $< 0.1\,\mathrm{ng\,m^{-3}}$ and allowed discernment of GEM peaks from the baseline noise for all measurements, also in Basel when the sampling time share for up- and downdraft was low during less turbulent conditions due to the fixed deadband.

The method detection limit was derived in the field from sampling the same air through updraft and downdraft lines (Fig. 5). The assessment of this bias between the sampling lines during the Basel measurements revealed an elevated SD of the offset between cartridges 1 and 3 (Fig. 6, blue line). Swapping of the sampling lines and exchange of the gold cartridges confirmed a mechanical problem originating from Teflon isolation valves. For this reason measurements with cartridge pair 1–3 were discarded for both campaigns.

A minimum detectable GEM concentration difference based on 1σ was derived from individual sampling line bias measurements for Basel ($0.01\,\mathrm{ng\,m^{-3}}$) and Degerö ($0.06\,\mathrm{ng\,m^{-3}}$) (Sect. 2.4.3). Thus, 98 % of the available 30 min data in Basel and 62 % at Degerö were above that limit. Zhu et al. (2015b) reported that 55 % of their Hg-REA flux data were significantly different from zero. Data from bias determination for cartridge-pair 2–4 did not reveal any significant diurnal pattern or trend over time for both sites (Fig. 6, red line).

AMTD
8, 8113–8156, 2015

3.1.4 Data coverage

Based on a systematic bias when using the cartridge-pair 1–3, 50 % of the data from Basel and 52 % from Degerö were discarded (Table 1). Some of the remaining flux measurements were rejected due to logging failures including power breakdowns. 6 % of the data at Basel and 4 % at Degerö were rejected due to poorly developed turbulence, determined by applying an integral turbulent characteristics test (Sect. 2.4.3). GEM flux measurements during extremely stable conditions were omitted ($z/L > 2$). The data were also screened for irregularities in the measured sampling air flow (deviation from the flow setting value > 2.5 %). Dry Hg-free air was used to determine possible cartridge or sampling line contamination and to discard periods of a noisy Hg detector baseline, due to rapid temperature changes within the detector box. Flux measurements were discarded if the signal of the blank measurements exceeded 10 % of the integration peak area that is detected for Hg in ambient air. In other Hg-REA studies, 44 % (Sommar et al., 2013a) and 28 % (Zhu et al., 2015b) of the data were flagged as moderate and low data quality due to turbulence characteristics (cf. Mauder and Foken, 2004). In our study the overall half hourly data loss was, 62 % at Basel and 68 % at Degerö.

3.2 Meteorological conditions

During the measurements in Basel temperatures averaged $-7.9 \pm 3.3\,^{\circ}\mathrm{C}$ (±SD). Precipitation occurred in the first two days and caused substantial loss of EC data, while GEM flux determination was not affected. From 3–12 February 2012, measurements were done during predominantly cloudless conditions with daily solar radiation (Rg) peaks between 300–500 $\mathrm{W\,m^{-2}}$. Relative humidity ranged between 20 and 91 % and was on average significantly lower in Basel than at Degerö. Wind speed in Basel averaged 2.6 $\mathrm{m\,s^{-1}}$ and did not differ significantly between day ($\mathrm{Rg} > 5\,\mathrm{W\,m^{-2}}$) and night ($\mathrm{Rg} < 5\,\mathrm{W\,m^{-2}}$). Wind direction was predominantly from northwest during the day and southeast during the night (Fig. S3b). Unstable atmospheric stratification ($z/L < -0.05$)

AMTD
8, 8113–8156, 2015

was predominant (92 % of time) during the Basel campaign while less than 3 % of the measurements were conducted during stable conditions ($z/L > 0.05$).

The campaign on the boreal mire commenced on 5 May 2012. The surface was covered by maximum of 33 cm snow which melted away towards the end of the campaign on 24 May 2012. A total precipitation amount of 19.6 mm was recorded during the campaign including a heavy snowfall during the morning of 6 May. Air temperatures averaged 5.4 ± 3.5 °C, whereas daily averages increased from 0.0 to 9.1 °C over the period. Soil temperatures at 2 cm depth likewise increased from 3.2 to 8.0 °C (daily averages). The prevailing wind direction at Degerö was from northeast to south with an average wind speed at 2.9 m s^{-1} (daytime mean: 3.1 m s^{-1}, nighttime mean: 2.1 m s^{-1}) (Fig. S3d). Conditions were stable ($z/L > 0.02$) 22 % of the time (daytime: 15 %, nighttime: 43 %), unstable for another 38 % (daytime: 42 %, nighttime: 22 %) ($z/L < -0.02$) and neutral during the remaining 40 % (daytime: 43 %, nighttime: 34 %).

3.3 Footprint and turbulence regime

In Basel the GEM flux measurements were conducted over a rough surface showing strongly modified vertical turbulent exchange processes. Measurements were conducted within the inertial sublayer, which overlays the urban roughness sublayer assuming that the upper level of the roughness sublayer is about two times the average building height of 17 m (Feigenwinter et al., 2012). 90 % of the GEM fluxes measured in Basel originated from a source area that covered 78 ha and reflected a blended, spatially averaged signal (Fig. 7a). Within that footprint the water fraction accounts for 7 %, the vegetation fraction for 19 %, the building fraction for 36 % and impervious ground surface for 38 %. Main wind directions during the campaign mimicked the dominant seasonal wind direction from NNW and ESE.

An inspection of the normalized co-spectra for sensible heat, latent heat and CO_2 flux revealed the occurrence of large eddies leading to comparably low switching intervals of 1.4 ± 0.3 Hz (mean ± SD). The co-spectral estimates were derived from 20 Hz data over the entire campaign during instable conditions and demonstrate that high-

AMTD
8, 8113–8156, 2015

frequency losses for sensible heat, latent heat and CO_2 fluxes were minimal. Low-frequency losses resulted due to the applied high-pass filter which attenuated fluctuations at periods larger than the time constant of 16.6 min (RF in Fig. 8). Ogives were calculated after Foken et al. (2012) and converged at approximately 90 % of all cases within the 30 min averaging period (Fig. 8a). Simulated damping factors for REA fluxes revealed that at mean wind speed of 2.6 m s^{-1} less than 10 % of the flux was dampened (Fig. 4a). We conclude that applying a 30 min averaging interval, a high-pass filter and valve switching at 10 Hz was adequate for REA flux calculations since considerable flux damping occurs just at low frequency ranges, instable conditions and low wind velocities (Figs. S4a and S5a).

90 % of the flux source area at Degerö comprised 0.6 ha (Fig. 7b). For all contour lines calculated, the mire surface was physically homogenous. The roughness length z_0 present during the campaign was only a few millimeters due to the short vegetation (Sagerfors et al., 2008) and negligible when there was snow-cover. During the Degerö campaign, the normalized turbulence spectra and ogives were derived for sensible heat flux during unstable conditions (Fig. 8b). Due to technical problems regarding the LI-6262 closed-path infrared gas analyzer, CO_2 and latent heat flux data were not used for spectral analysis. In comparison to Basel the co-spectrum of the sensible heat flux was shifted significantly towards higher frequencies. The occurrence of more smaller eddies increased the fast-response valve switching interval (2.9 ± 0.7 Hz; mean ± SD) which increased with increasing u_* (Fig. S6). High frequency losses at 10 Hz accounted for less than 5 % of the sensible heat flux. The ogive converged a constant value at RF and indicates that large eddies were sampled completely over the averaging period (Fig. 8b). At Degerö the integral damping factor for the REA flux was more than 20 % at high frequencies especially during stable and strong wind conditions (Figs. S4b and S5b).

AMTD
8, 8113–8156, 2015

3.4 GEM concentrations

Mean ± SD atmospheric GEM concentration in Basel was $4.1 \pm 0.8\,\mathrm{ng\,m^{-3}}$. The average concentration difference between up and downdraft was $0.24 \pm 0.2\,\mathrm{ng\,m^{-3}}$ (median: $0.18\,\mathrm{ng\,m^{-3}}$) (Fig. 9). We suggest that during the exceptionally cold period in Basel gas and oil-fired thermal power stations within the dense urban source area contributed to enhanced GEM concentrations. Highest GEM levels were observed during periods of low wind velocities ($u_* < 0.3\,\mathrm{m\,s^{-1}}$) and southern wind directions (Fig. S3a). Most likely additional GEM emissions from vehicular traffic along a highly frequented road contributed to observed elevated Hg concentrations during southerlies. The road runs in a north/south direction and is the major source of CO_2 (Lietzke and Vogt, 2013).

The average air concentration during snowmelt at Degerö was $1.6 \pm 0.2\,\mathrm{ng\,m^{-3}}$, comparable to observations made in 2009 by static chambers (Fritsche et al., 2014). Concentration difference in REA conditional samples collected at Degerö averaged $0.13 \pm 0.2\,\mathrm{ng\,m^{-3}}$ (median: $0.1\,\mathrm{ng\,m^{-2}}$) which is about a factor of two lower than the magnitude observed in Basel (Fig. 9). No significant concentration relationships were found with either wind direction (Fig. S3c) or atmospheric stability.

3.5 GEM flux estimation in contrasting environments

Urban areas are of particular concern with respect to the global Hg cycle. Industrial sectors and anthropogenic combustion processes emit large quantities of Hg to the atmosphere (Walcek et al., 2003) wherefrom mostly divalent mercury (Hg(II)) and particulate-bound mercury (PHg) deposit locally. Highly variable Hg air concentrations, the physically and chemically diverse nature of urban surface covers and urban meteorology (e.g. heat island effect) are suggested to create complex Hg flux patterns above cities (Gabriel et al., 2005). Up to now, just a handful of studies have described GEM emissions from urban environments (Kim and Kim, 1999; Feng et al., 2005; Obrist et al., 2006; Eckley and Branfireun, 2008; Gabriel et al., 2006). GEM fluxes measured in Basel showed a diurnal trend with a maximum deposition around noon and high-

AMTD
8, 8113–8156, 2015

est emissions around 7 p.m. (Fig. 10a). The mean flux ± SE of $15.4 \pm 13.3\,ng\,m^{-2}\,h^{-1}$ indicated that this urban area was a net source of atmospheric Hg during the study period. Similarly, for the same site in spring and fall, Obrist et al. (2006) observed average GEM emissions of $6.5 \pm 0.9\,ng\,m^{-2}\,h^{-1}$ (± SD) in the stable nocturnal boundary layer using the $Rn222/Hg^0$ method. Environmental conditions such as solar radiation, air and soil temperature are known to be major drivers of natural GEM emission (e.g. Schroeder et al., 1989; Steffen et al., 2002; Choi and Holsen, 2009). North westerly wind directions were associated with GEM deposition between 2 a.m. and 1 p.m. In contrast, emission events were linked to wind directions from the south east.

Determination of GEM snow-air exchange has been a subject of interest since the first atmospheric mercury depletion events (AMDEs) were observed (Schroeder et al., 1998). Non-arctic GEM flux studies from snowpack report deposition as well as emission events with near zero net fluxes (Faïn et al., 2007; mean: $0.4\,ng\,m^{-2}\,h^{-1}$; Fritsche et al., 2008b; mean: $0.3\,ng\,m^{-2}\,h^{-1}$).

The mean GEM snow-air transfer observed at Degerö was $3.0 \pm 3.8\,ng\,m^{-2}\,h^{-1}$ (±SE). It is the result of a balance between deposition prevailing from midnight to noon and vice versa during the rest of the day when emission predominates (Fig. 10b). REA fluxes varied strongly during both the day and night but revealed a significant difference between GEM fluxes during unstable (median: $8.7\,ng\,m^{-2}\,h^{-1}$), stable (median: $-0.1\,ng\,m^{-2}\,h^{-1}$) and neutral conditions (median: $-4\,ng\,m^{-2}\,h^{-1}$) (Mann–Whitney U test, $p < 0.05$). GEM concentrations in the surface snow layers were not determined in this study but in accordance with Faïn et al. (2013), GEM is likely enhanced during the course of daytime compared to ambient air due to sunlight-mediated processes. An impact of fresh snowfall and possible wet Hg deposition on GEM fluxes could not be observed with REA but precipitation events occurred regularly in the afternoon and might have contributed to GEM volatilized in the evenings together with GEM produced during dusk and night (Faïn et al., 2013).

GEM flux quantification compared to previous systems is improved due to the synchronous sampling, and the monitoring of regular GEM reference concentration and

AMTD
8, 8113–8156, 2015

dry, Hg-free air. As demonstrated here, these improvements make REA feasible for measurements over tall buildings but also short vegetation and snow-cover. At Degerö, however, higher abundance of smaller eddies increased the GEM flux variability. However, the REA technique remains better suited to assessing magnitudes and variability of fluxes rather determining the effects of short-term variability in environmental parameters on GEM fluxes (cf. Gustin et al., 1999).

For future long-term REA applications we have three suggestions: (i) a more regular determination of the bias between both sampling lines. Either by a weekly check of the bias or by implementing an additional valve to switch up- and downdraft lines every hour (each cartridge would measure up- and downdraft). (ii) Hg detector sensitivity due to rapid temperature changes are corrected for but could be avoided to a large extent by using a more effective temperature control unit. (iii) To improve the accuracy in the air volumes sampled by installing mass flow meters for up- and downdraft lines.

4 Conclusions

The need to precisely determine land–atmosphere exchange over long continuous periods is widely recognized (Schwartzendruber and Jaffe, 2012). REA has the potential to do this more effectively than other methods. Therefore, several REA systems have been deployed, but their accuracy has been impaired by several design features such as the use of multiple detectors and non-synchronous sample collection. We developed a dual inlet, single analyzer system that has overcome these shortcomings and included new features such as the integrated GEM reference and a filtered zero-air unit for semi-continuous monitoring of GEM recovery, as well as blank measurements. The data acquisition and control system is fully automated and could be remotely controlled which reduces the workload compared to other REA systems. We have demonstrated the system in contrasting environments to measure turbulent transport of GEM 38 m a.g.l. in Basel, Switzerland and 1.8 m above a snow covered boreal mire in Sweden. While the demonstration identified room for further improvements, we

AMTD
8, 8113–8156, 2015

believe this novel design has the potential to facilitate the use of REA for measuring land–atmosphere Hg exchange for sustained periods in a variety of environments.

The Supplement related to this article is available online at doi:10.5194/amtd-8-8113-2015-supplement.

Acknowledgements. This research was funded by the Swedish Research Council (2009-15586-68819-37), the Department of Earth Sciences, Uppsala University, and the Department of Environmental Geosciences, University of Basel. We thank William Larsson and the late Lars Lundmark from Umeå University for technical assistance and engineering, Roland Vogt from the University of Basel's MCR lab for using their EC setup. The study at Degerö Stormyr also received technical and maintenance support from the Svartberget Experimental Forest, Vindeln, Sweden. The study was also supported by the Swedish research infrastructures, ICOS Sweden (Integrated Carbon Observatory System) and SITES (Swedish Infrastructure for Ecosystem Science) at Degerö Stormyr, both partly financed by the Swedish Research Council.

References

Åkerblom, S., Bishop, K., Bjorn, E., Lambertsson, L., Eriksson, T., and Nilsson, M. B.: Significant interaction effects from sulfate deposition and climate on sulfur concentrations constitute major controls on methylmercury production in peatlands, Geochim. Cosmochim. Ac., 102, 1–11, 2013.

Alexandersson, H., Karlström, C., and Larsson-McCann, S.: Temperaturen och nederbörden i Sverige 1961–1990, The Swedish Meteorological and Hydrological Institute, Norrköping, Sweden, 1991.

Ammann, C.: On the applicability of Relaxed Eddy Accumulation and Common Methods for Measuring Trace Gas Fluxes, PhD Thesis, ETH Zürich, Zürich, 229 pp., 1999.

Ammann, C. and Meixner, F. X.: Stability dependence of the relaxed eddy accumulation coefficient for various scalar quantities, J. Geophys. Res., 107, 4071, doi:10.1029/2001JD000649, 2002.

AMTD
8, 8113–8156, 2015

Arnts, R. R., Mowry, F. L., and Hampton, G. A.: A high-frequency response relaxed eddy accumulation flux measurement system for sampling short-lived biogenic volatile organic compounds, J. Geophys. Res.-Atmos., 118, 4860–4873, 2013.
Baker, J. M., Norman, and Bland, W. L.: Field-scale application of flux measurement by conditional sampling, Agric. Forest Meteorol., 62, 31–52, 1992.
Bash, J. O. and Miller, D. R.: A note on elevated total gaseous mercury concentrations downwind from an agriculture field during tilling, Sci. Total Environ., 388, 379–388, 2007.
Bash, J. O. and Miller, D. R.: A relaxed eddy accumulation system for measuring surface fluxes of total gaseous mercury, J. Atmos. Ocean. Tech., 25, 244–257, 2008.
Bash, J. O. and Miller, D. R.: Growing season total gaseous mercury (TGM) flux measurements over an *Acer rubrum* L. stand, Atmos. Environ., 43, 5953–5961, 2009.
Bauer, D., Campuzano-Jost, P., and Hynes, A. J.: Rapid, ultrasensitive detection of gas phase elemental mercury under atmospheric conditions using sequential two-photon laser induced fluorescence, J. Environ. Monitor., 4, 339–343, 2002.
Brut, A., Legain, D., Durand, P., and Laville, P.: A relaxed eddy accumulator for surface flux measurements on ground-based platforms and aboard research vessels, J. Atmos. Ocean. Tech., 21, 411–427, 2004.
Businger, J.: Evaluation of the accuracy with which dry deposition can be measured with current micrometeorological techniques, J. Clim. Appl. Meteorol., 25, 1100–1124, 1986.
Choi, H.-D. and Holsen, T. M.: Gaseous mercury fluxes from the forest floor of the Adirondacks, Environ. Pollut., 157, 592–600, 2009.
Cobos, D. R., Baker, J. M., and Nater, E. A.: Conditional sampling for measuring mercury vapor fluxes, Atmos. Environ., 36, 4309–4321, 2002.
Converse, A. D., Riscassi, A. L., and Scanlon, T. M.: Seasonal variability in gaseous mercury fluxes measured in a high-elevation meadow, Atmos. Environ., 44, 2176–2185, 2010.
Desjardins, R. L.: A study of Carbon Dioxide and Sensible Heat Fluxes using the Eddy Correlation Technique, PhD Thesis, Cornell University, Ithaca, 189 pp., 1972.
Desjardins, R. L.: Energy budget by an eddy correlation method, J. Appl. Meteorol., 16, 248–250, 1977.
Eckley, C. S. and Branfireun, B.: Gaseous mercury emissions from urban surfaces: controls and spatiotemporal trends, Appl. Geochem., 23, 369–383, 2008.
Faïn, X., Grangeon, S., Bahlmann, E., Fritsche, J., Obrist, D., Dommergue, A., Ferrari, C. P., Cairns, W., Ebinghaus, R., Barbante, C., Cescon, P., and Boutron, C.: Diurnal production of

AMTD
8, 8113–8156, 2015

gaseous mercury in the alpine snowpack before snowmelt, J. Geophys. Res., 112, D21311, doi:10.1029/2007JD008520, 2007.
Faïn, X., Moosmüller, H., and Obrist, D.: Toward real-time measurement of atmospheric mercury concentrations using cavity ring-down spectroscopy, Atmos. Chem. Phys., 10, 2879–2892, doi:10.5194/acp-10-2879-2010, 2010.
Faïn, X., Helmig, D., Hueber, J., Obrist, D., and Williams, M. W.: Mercury dynamics in the Rocky Mountain, Colorado, snowpack, Biogeosciences, 10, 3793–3807, doi:10.5194/bg-10-3793-2013, 2013.
Feigenwinter, C., Vogt, R., and Christen, A.: Eddy covariance measurements over urban areas, in: Eddy Covariance – a Practical Guide to Measurement and Data Analysis, edited by: Aubinet, M., Vesala, T., and Papale, D., Springer Science+Business Media B.V., Dordrecht, the Netherlands, 377–397, 2012.
Feng, X. B., Wang, S. F., Qiu, G. A., Hou, Y. M., and Tang, S. L.: Total gaseous mercury emissions from soil in Guiyang, Guizhou, China, J. Geophys. Res.-Atmos., 110, D14306, doi:10.1029/2004JD005643, 2005.
Foken, T.: Angewandte Meteorologie, Mikrometeorologische Methoden, 2. Auflage, Springer, Berlin, 2006.
Foken, T. and Wichura, B.: Tools for quality assessment of surface-based flux measurements, Agr. Forest Meteorol., 78, 83–105, 1996.
Foken, T., Leuning, R., Oncley, S. R., Mauder, M., and Aubinet., M.: Corrections and data quality control, in: Eddy Covariance – a Practical Guide to Measurement and Data Analysis, edited by: Aubinet, M., Vesala, T., and Papale, D., Springer Science+Business Media B.V., Dordrecht, the Netherlands, 85–131, 2012.
Fritsche, J.: Air–Surface Exchange of Elemental Mercury in Uncontaminated Grasslands. Determination of Fluxes and Identification of Forcing Factors with Micrometeorological Methods and Controlled Laboratory Studies, PhD Thesis, University of Basel, Basel, 95 pp., 2008.
Fritsche, J., Obrist, D., Zeeman, M. J., Conen, F., Eugster, W., and Alewell, C.: Elemental mercury fluxes over a sub-alpine grassland determined with two micrometeorological methods, Atmos. Environ., 42, 2922–2933, 2008a.
Fritsche, J., Wohlfahrt, G., Ammann, C., Zeeman, M., Hammerle, A., Obrist, D., and Alewell, C.: Summertime elemental mercury exchange of temperate grasslands on an ecosystem-scale, Atmos. Chem. Phys., 8, 7709–7722, doi:10.5194/acp-8-7709-2008, 2008b.

AMTD
8, 8113–8156, 2015

Fritsche, J., Osterwalder, S., Nilsson, M. B., Sagerfors, J., Åkerblom, S., Bishop., K., and Nilsson., M.: Evasion of elemental mercury from a boreal peatland suppressed by long-term sulfate addition, Environ. Sci. Technol., 1, 421–425, 2014.

Gabriel, M. C., Williamson, D., Lindberg, S., Zhang, H., and Brooks, S.: Spatial variability of total gaseous mercury emission from soils in a southeastern US urban environment, Environ. Geol., 48, 955–964, 2005.

Gabriel, M. C., Williamson, D. G., Zhang, H., Brooks, S., and Lindberg, S.: Diurnal and seasonal trends in total gaseous mercury flux from three urban ground surfaces, Atmos. Environ., 40, 4269–4284, 2006.

Gaman, A., Rannik, Ü., Aalto, P., Pohja, T., Siivola, E., Kulmala, M., and Vesala, T.: Relaxed eddy accumulation system for size-resolved aerosol particle flux measurements, J. Atmos. Ocean. Tech., 21, 933–943, 2004.

Granberg, G., Sundh, I., Svensson, B. H., and Nilsson, M.: Effects of temperature, and nitrogen and sulfur deposition, on methane emission from a boreal mire, Ecology, 82, 1982–1998, 2001.

Grigal, D. F.: Inputs and outputs of mercury from terrestrial watersheds: a review, Environ. Rev., 10, 1–39, 2002.

Grönholm, T., Haapanala, S., Launiainen, S., Rinne, J., Vesala, T., and Rannik, Ü.: The dependence of the beta coefficient of REA system with dynamic deadband on atmospheric conditions, Environ. Pollut., 152, 597–603, 2008.

Gustin, M. S.: Exchange of mercury between the atmosphere and terrestrial ecosystems, in: Advances in Environmental Chemistry, and Toxicology of Mercury, edited by: Cai, Y., Liu, G., and O'Driscoll, N. J., John Wiley & Sons, Hoboken, NJ, USA, 423–452, 2011.

Gustin, M. S. and Lindberg, S. E.: Terrestrial Hg fluxes: is the next exchange up, down, or neither?, in: Dynamics of Mercury Pollution on Regional and Global Scales, edited by: Pirrone, N. and Mahaffey, K. R., Springer, New York, 241–259, 2005.

Gustin, M. S., Lindberg, S., Marsik, F., Casimir, A., Ebinghaus, R., Edwards, G., Hubble-Fitzgerald, C., Kemp, R., Kock, H., Leonard, T., London, J., Majewski, M., Montecinos, C., Owens, J., Pilote, M., Poissant, L., Rasmussen, P., Schaedlich, F., Schneeberger, D., Schroeder, W., Sommar, J., Turner, R., Vette, A., Wallschlaeger, D., Xiao, Z., and Zhang, H.: Nevada STORMS project: measurement of mercury emissions from naturally enriched surfaces, J. Geophys. Res.-Atmos., 104, 21831–21844, 1999.

AMTD
8, 8113–8156, 2015

Gustin, M. S., Lindberg, S. E., Austin, K., Coolbaugh, M., Vette, A., and Zhang, H.: Assessing the contribution of natural sources to regional atmospheric mercury budgets, Sci. Total Environ., 259, 61–71, 2000.
Gustin, M. S., Lindberg, S. E., and Weisberg, P. J.: An update on the natural sources and sinks of atmospheric mercury, Appl. Geochem., 23, 482–493, 2008.
Haapanala, S., Rinne, J., Pystynen, K.-H., Hellén, H., Hakola, H., and Riutta, T.: Measurements of hydrocarbon emissions from a boreal fen using the REA technique, Biogeosciences, 3, 103–112, doi:10.5194/bg-3-103-2006, 2006.
Hensen, A., Nemitz, E., Flynn, M. J., Blatter, A., Jones, S. K., Sørensen, L. L., Hensen, B., Pryor, S. C., Jensen, B., Otjes, R. P., Cobussen, J., Loubet, B., Erisman, J. W., Gallagher, M. W., Neftel, A., and Sutton, M. A.: Inter-comparison of ammonia fluxes obtained using the Relaxed Eddy Accumulation technique, Biogeosciences, 6, 2575–2588, doi:10.5194/bg-6-2575-2009, 2009.
Keeler, G. J. and Landis, M. S.: Standard Operating Procedure for Sampling Vapor Phase Mercury, University of Michigan, USA, 1994
Kim, K. H. and Kim, M. Y.: The exchange of gaseous mercury across soil–air interface in a residential area of Seoul, Korea, Atmos. Environ., 33, 3153–3165, 1999.
Kim, K.-H., Lindberg, S. E., and Meyers, T. P.: Micrometeorological measurements of mercury vapor fluxes over background forest soils in eastern Tennessee, Atmos. Environ., 29, 267–282, 1995.
Kormann, R. and Meixner, F. X.: An analytical footrpint model for non-neutral stratification, Bound.-Lay. Meteorol., 99, 207–224, 2001.
Lee, X. H.: Water vapor density effect on measurements of trace gas mixing ratio and flux with a massflow controller, J. Geophys. Res.-Atmos., 105, 17807–17810, 2000.
Lietzke, B. and Vogt, R.: Variability of CO_2 concentrations and fluxes in and above an urban street canyon, Atmos. Environ., 74, 60–72, 2013.
Lindberg, S. and Meyers, T.: Development of an automated micrometeorological method for measuring the emission of mercury vapor from wetland vegetation, Wetl. Ecol. Manag., 9, 333–347, 2001.
Lindberg, S., Bullock, R., Ebinghaus, R., Engstrom, D., Feng, X., Fitzgerald, W., Pirrone, N., and Seigneur, C.: A synthesis of progress and uncertainties in attributing the sources of mercury in deposition, Ambio, 36, 19–32, 2007.

AMTD
8, 8113–8156, 2015

Mason, R. P. and Sheu, G.-R.: Role of the ocean in the global mercury cycle, Global Biogeochem. Cy., 16, 1093, doi:10.1029/2001GB001440, 2002.
Mauder, M. and Foken, T.: Documentation and Instruction Manual of the Eddy Covariance Software Package TK2, vol. 26, Arbeitsergebnisse, Universitat Bayreuth, Abteilung Mikrometeorologie, Bayreuth, 42 pp., ISSN 1614–8916, 2004.
Mcmillen, R.: An Eddy-correlation technique with extended applicability to non-simple terrain, Bound.-Lay. Meteorol., 43, 231–245, 1988.
MeteoSchweiz: Klimanormwerte Basel/Binningen, Normperiode 1961–1990, available at: http://www.meteoschweiz.admin.ch/product/output/climate-data/climate-diagrams-normal-values-station-processing/BAS/climsheet_BAS_np6190_d.pdf (last access: 29 July 2015), 2014.
Meyers, T. P., Hall, M. E., Lindberg, S. E., and Kim, K.: Use of the modified Bowen-ratio technique to measure fluxes of trace gases, Atmos. Environ., 30, 3321–3329, 1996.
Meyers, T. P., Luke, W. T., and Meisinger, J. J.: Fluxes of ammonia and sulfate over maize using relaxed eddy accumulation, Agr. Forest Meteorol., 136, 203–213, 2006.
Milne, R., Beverland, I. J., Hargreaves, K., and Moncrieff, J. B.: Variation of the β coefficient in the relaxed eddy accumulation method, Bound.-Lay. Meteorol., 93, 211–225, 1999.
Milne, R., Mennim, A., and Hargreaves, K.: The value of the beta coefficient in the relaxed eddy accumulation method in terms of fourth-order moments, Bound.-Lay. Meteorol., 101, 359–373, 2001.
Moravek, A., Trebs, I., and Foken, T.: Effect of imprecise lag time and high-frequency attenuation on surface–atmosphere exchange fluxes determined with the relaxed eddy accumulation method, J. Geophys. Res.-Atmos., 118, 10210–10224, 2013.
Obrist, D., Conen, F., Vogt, R., Siegwolf, R., and Alewell, C.: Estimation of Hg^0 exchange between ecosystems and the atmosphere using ^{222}Rn and Hg^0 concentration changes in the stable nocturnal boundary layer, Atmos. Environ., 40, 856–866, 2006.
Olofsson, M., Ek-Olausson, B., Jensen, N. O., Langer, S., and Ljungström, E.: The flux of isoprene from a willow plantation and the effect on local air quality, Atmos. Environ., 39, 2061–2070, 2005a.
Olofsson, M., Sommar, J., Ljungstrom, E., Andersson, M., Wängberg, I.: Application of relaxed eddy accumulation technique to quantify Hg^0 fluxes over modified soil surfaces, Water Air Soil Pollut., 167, 331–352, 2005b.

AMTD
8, 8113–8156, 2015

Panofsky, H. A. and Dutton, J. A.: Atmospheric Turbulence – Models and Methods for Engineering Applications, Wiley, New York, 397 pp., 1984.
Peichl, M., Sagerfors, J., Lindroth, A., Buffam, I., Grelle, A., Klemedtsson, L., Laudon, H., and Nilsson, M. B.: Energy exchange and water budget partitioning in a boreal minerogenic mire, J. Geophys. Res.-Biogeo., 118, 1–13, 2013.
Pierce, A. M., Moore, C. W., Wohlfahrt, G., Hörtnagl, L., Kljun, N., and Obrist, D.: Eddy covariance flux measurements of gaseous elemental mercury using cavity ring-down spectroscopy, Environ. Sci. Technol., 49, 1559–1568, 2015.
Rannik, Ü., Markkanen, T., Raittila, J., Hari, P., and Vesala, T.: Turbulence statistics inside and over forest: influence on footprint prediction, Bound.-Lay. Meteorol., 109, 163–189, 2003.
Ren, X., Sanders, J. E., Rajendran, A., Weber, R. J., Goldstein, A. H., Pusede, S. E., Browne, E. C., Min, K.-E., and Cohen, R. C.: A relaxed eddy accumulation system for measuring vertical fluxes of nitrous acid, Atmos. Meas. Tech., 4, 2093–2103, doi:10.5194/amt-4-2093-2011, 2011.
Richardson, A. D., Aubinet, M., Barr, A. G., Hollinger, D. Y., Ibrom, A., Lasslop, G., and Reichstein, M.: Uncertainty quantification, in: Eddy Covariance – a Practical Guide to Measurement and Data Analysis, edited by: Aubinet, M., Vesala, T., and Papale, D., Springer Science+Business Media B.V., Dordrecht, the Netherlands, 173–209, 2012.
Sagerfors, J., Lindroth, A., Grelle, A., Klemedtsson, L., Weslien, P., and Nilsson, M.: Annual CO_2 exchange between a nutrient-poor, minerotrophic, boreal mire and the atmosphere, J. Geophys. Res.-Biogeo., 113, G01001, doi:10.1029/2006JG000306, 2008.
Schroeder, W. H., Lindquist, O., and Munthe, J.: Volatilisation of mercury from natural surfaces, Proc. 7th International Conference of Heavy Metals in the Environment, Geneva, Switzerland, September 1989, edited by: Vernet, J. P., CEP Consultants, Edinburgh, UK, 480–484, 1989.
Schroeder, W. H., Anlauf, K. G., Barrie, L. A., Lu, J. Y., Steffen, A., Schneeberger, D. R., and Berg, T.: Arctic springtime depletion of mercury, Nature, 394, 331–332, 1998.
Schwartzendruber, P. and Jaffe, D.: Sources and transport. A global issue, in: Mercury in the Environment: Pattern and Process, 1st edn., edited by: Bank, M. S., University of California Press, Berkely, CA, 3–18, 2012.
Shanley, J. B. and Bishop, K.: Mercury cycling in terrestrial watersheds, in: Mercury in the Environment: Pattern and Process, 1st edn., edited by: Bank, M. S., University of California Press, Berkely, CA, 119–141, 2012.

AMTD
8, 8113–8156, 2015

Skov, H., Brooks, S. B., Goodsite, M. E., Lindberg, S. E., Meyers, T. P., Landis, M. S., Larsen, M. R. B., Jensen, B., McConville, G., and Christensen, J.: Fluxes of reactive gaseous mercury measured with a newly developed method using relaxed eddy accumulation, Atmos. Environ., 40, 5452–5463, 2006.

Slemr, F., Brunke, E.-G., Ebinghaus, R., Temme, C., Munthe, J. Wängberg, I., Schroeder, W., Steffen, A., and Berg, T.: Worldwide trend of atmospheric mercury since 1977, Geophys. Res. Lett., 30, 1516, doi:10.1029/2003GL016954, 2003.

Sommar, J., Zhu, W., Shang, L., Feng, X., and Lin, C.-J.: A whole-air relaxed eddy accumulation measurement system for sampling vertical vapour exchange of elemental mercury, Tellus B, 65, 19940, doi:10.3402/tellusb.v65i0.19940, 2013a.

Sommar, J., Zhu, W., Lin, C.-J., and Feng, X.: Field approaches to measure Hg exchange between natural surfaces and the atmosphere – a review, Critical Reviews in Environ. Sci. Technol., 43, 1657–1739, 2013b.

Steffen, A., Schroeder, W. H., Bottenheim, J., Narayan, J., and Fuentes, J. D.: Atmospheric mercury concentrations: measurements and profiles near snow and ice surfaces in the Canadian Arctic during Alert 2000, Atmos. Environ., 36, 2653–2661, 2002.

United Nations Environment Programme: Minimata Convention on Mercury, available at: http://www.unep.org (last access: 29 July 2015), 31 pp., 2013a.

United Nations Environment Programme: Global Mercury Assessment 2013: Sources, Emissions, Releases and Environmental Transport, UNEP Chemicals Branch, Geneva, Switzerland, 2013b.

Walcek, C., De Santis, S., and Gentile, T.: Preparation of mercury emissions for eastern North America, Environ. Pollut., 123, 375–381, 2003.

Zhu, W., Sommar, J., Lin, C.-J., and Feng, X.: Mercury vapor air–surface exchange measured by collocated micrometeorological and enclosure methods – Part I: Data comparability and method characteristics, Atmos. Chem. Phys., 15, 685–702, doi:10.5194/acp-15-685-2015, 2015a.

Zhu, W., Sommar, J., Lin, C.-J., and Feng, X.: Mercury vapor air–surface exchange measured by collocated micrometeorological and enclosure methods – Part II: Bias and uncertainty analysis, Atmos. Chem. Phys., 15, 5359–5376, doi:10.5194/acp-15-5359-2015, 2015b.

AMTD
8, 8113–8156, 2015

Table 1. Overview of rejection criteria for the evaluation of REA field measurements. Rejected amount of data (%) and remaining numbers of observations (n) are given.

Criterion	Basel	Degerö
	Rejection percentage	
cartridge-pair offset	52 %	50 %
logging failure	4 %	7 %
insufficient turbulence (σ_w/u_*)	6 %	4 %
extreme stability ($z/L > 2$)	0 %	0 %
sampling air flow and blank irregularities	1 %	4 %
Total rejection (excl. cartridge-pair offset)	12 %	16 %
Remaining observations	$n = 287$	$n = 375$

AMTD
8, 8113–8156, 2015

Table 2. Summary of averaged, median and distribution of GEM fluxes, GEM concentrations and environmental conditions during the measurement campaigns. Pearson correlation coefficients (r) between GEM flux and environmental parameters are given if statistically significant ($p < 0.05$).

Variable	unit	Basel Mean	Median	10th/90th percentile	r	Degerö Mean	Median	10th/90th percentile	r
GEM flux	ng m^{-2} h^{-1}	15.4	34.9	−262/270		3.0	2.6	−71/67	–
GEM concentration	ng m^{-3}	4.1	3.9	3.3/5.2		1.6	1.6	1.4/1.8	–
Sensible heat flux (EC)	Wm^{-2}	73	65	20/134		12	2.5	−17/58	**0.15**
Latent heat flux (EC)	Wm^{-2}	12	11	1.8/25	**0.39**	–	–	–	–
CO_2 flux (EC)	µmol m^{-2} s^{-1}	0.02	0.01	0/0.05	**0.39**	–	–	–	–
Friction velocity	m s^{-1}	0.41	0.38	0.2/0.7	**0.2**	0.19	0.18	0.07/0.3	**−0.2**
Wind speed	m s^{-1}	2.6	2.5	1.3/3.9		2.9	2.7	1.0/4.8	**−0.28**
Solar radiation	Wm^{-2}	78	–	0/312	**−0.29**	159	–	0/455	–
Air temperature	°C	−7.9	−8	−12.0/3.4	**0.29**	5.3	5.4	0.1/10.2	**0.3**
Soil temperature	°C [2 cm]	–	–	–		6.7	7	4.4/8.2	**0.3**
Relative humidity	%	62	60	40/85	**−0.28**	76	80	47/98	**−0.19**

AMTD
8, 8113–8156, 2015

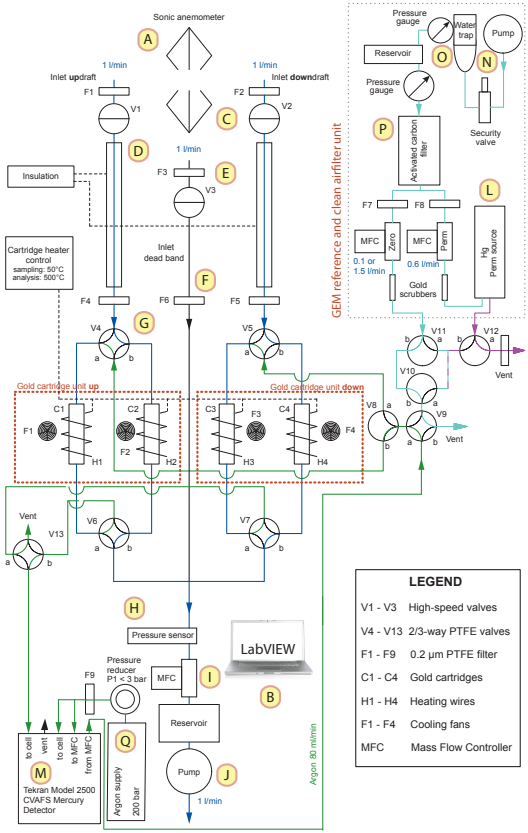

Figure 1. Schematic of the REA system hardware. It consists of a GEM sampling unit, a GEM reference and clean airfilter unit (upper right). Capital letters refer to REA components mentioned in the text and described in Table S1. The air volume drawn over the gold cartridges equaled 1 L min^{-1} in Basel and 1.5 L min^{-1} at Degerö.

AMTD
8, 8113–8156, 2015

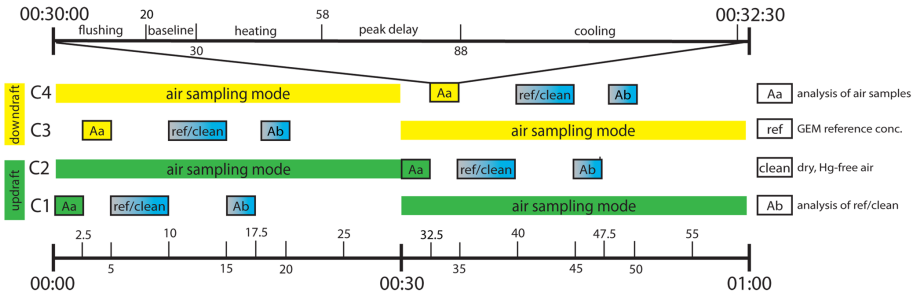

Figure 2. The hourly measuring cycle of the REA system subdivided into the air sampling and GEM analysis procedures (Aa, ref/clean, Ab). At the start of a sequence, cartridge-pair C2 and C4 adsorb GEM in the up- and downdraft simultaneously while previously adsorbed GEM from cartridges C1 and C3 is analyzed. During each cycle, eight analysis procedures which last for 2.5 min were conducted.

AMTD
8, 8113–8156, 2015

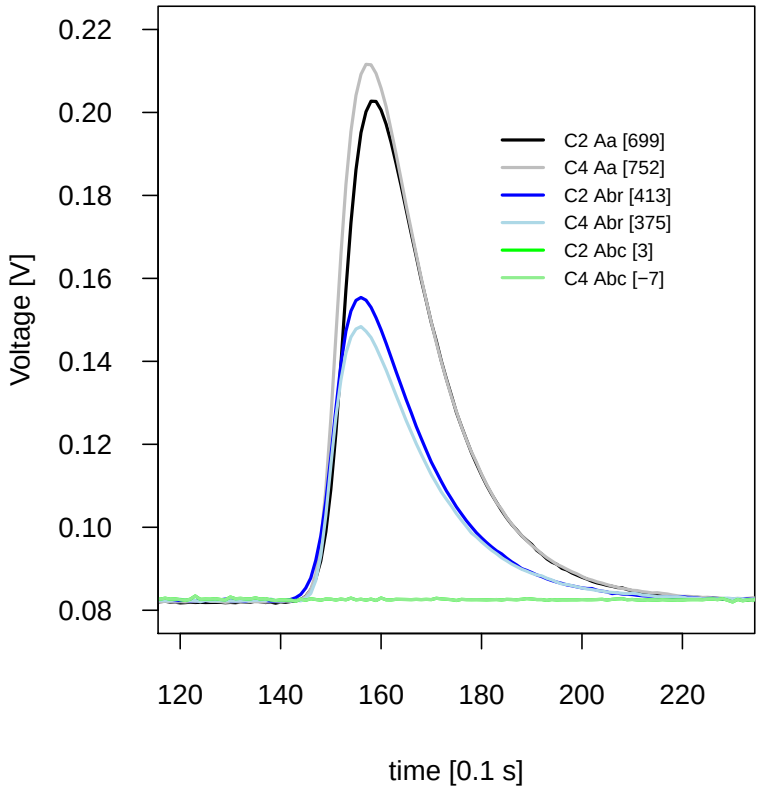

Figure 3. Representative peak recovery for all 4 cartridges during ambient air (Aa), GEM reference air (Ab_r), and dry, Hg-free air measurements (Ab_c) on 11 February 2012, between 14:00 and 15:30 LT in Basel. The plots show an extract of 10 s from the peak delay sequence which takes 30 s in total. *Y* axis indicates the Hg detector baseline voltage [V].

AMTD
8, 8113–8156, 2015

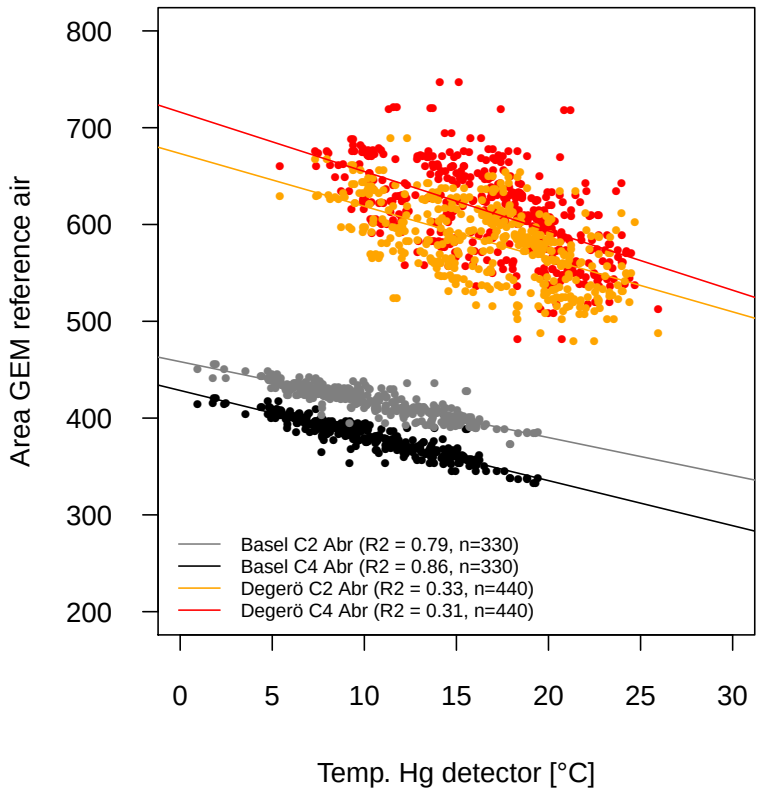

Figure 4. Linear relationship between GEM reference air for up- and downdraft in Basel (grey, black) and Degerö (orange, red), respectively and ambient temperatures within the Hg detector box.

AMTD
8, 8113–8156, 2015

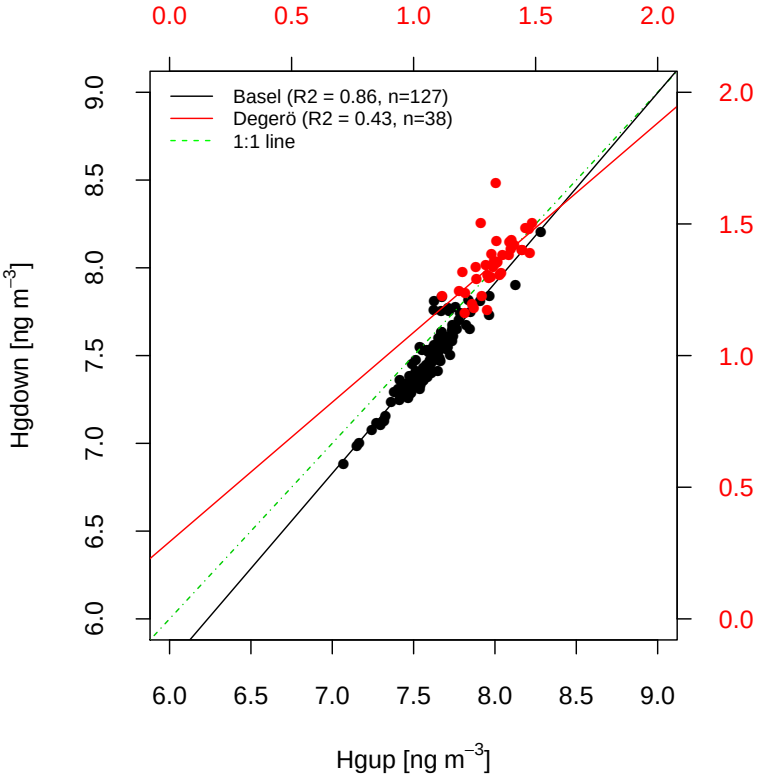

Figure 5. Results from conditional channel inter-comparison campaigns at Basel (black) and Degerö (red) for cartridge-pair 2–4.

AMTD
8, 8113–8156, 2015

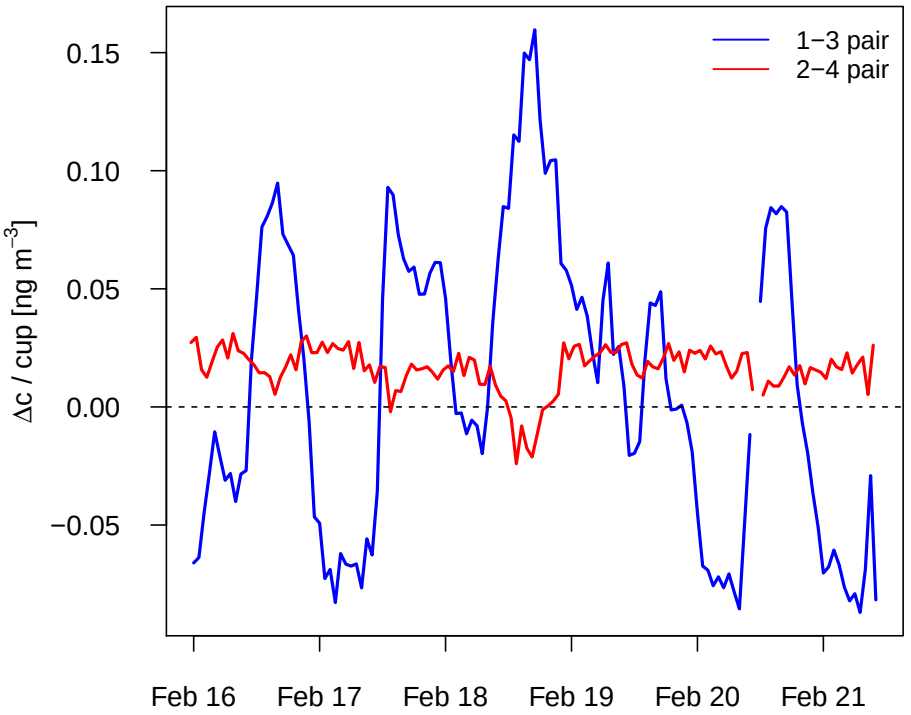

Figure 6. Precision in concentration difference measurements of the Hg standard between cartridge pair 2–4 (red) and 1–3 (blue). The measurements were conducted between 16 February, 00:00:00 LT and 21 February 2012, 12:00:00 LT in Basel.

AMTD
8, 8113–8156, 2015

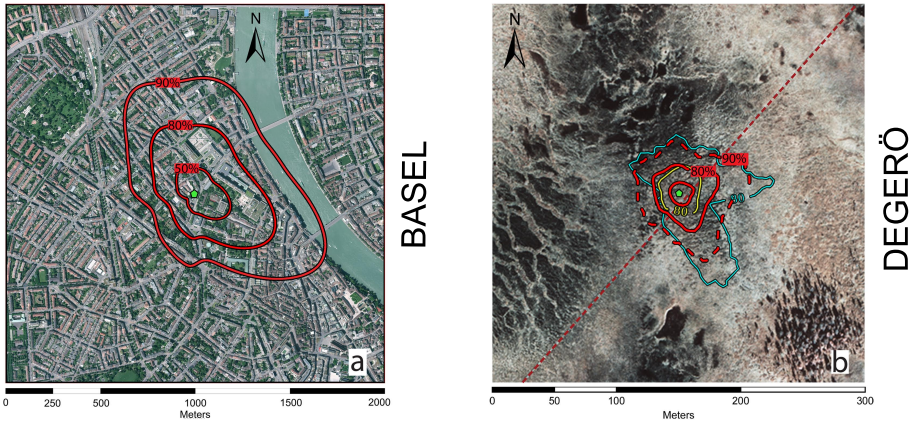

Figure 7. Aerial RGB and IR photographs with red contours containing 50, 80 and 90 % of the flux during the campaign in Basel **(a)** and Degerö **(b)**. The yellow and blue 80 %-contours at Degerö stand for instable and stable conditions, respectively. The light-green Pentagon indicates the location of the flux tower.

AMTD
8, 8113–8156, 2015

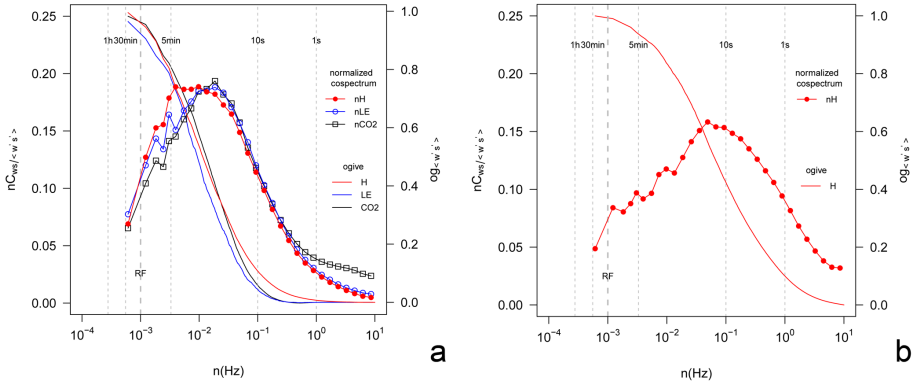

Figure 8. Normalized turbulence co-spectra (y axis, lines + symbols) and converging ogives (secondary y axis, lines) of sensible heat (red), latent heat (blue) and CO_2 flux (black) during instable conditions for Basel **(a)** and Degerö **(b)**. At Degerö only high resolution temperature data were used.

AMTD
8, 8113–8156, 2015

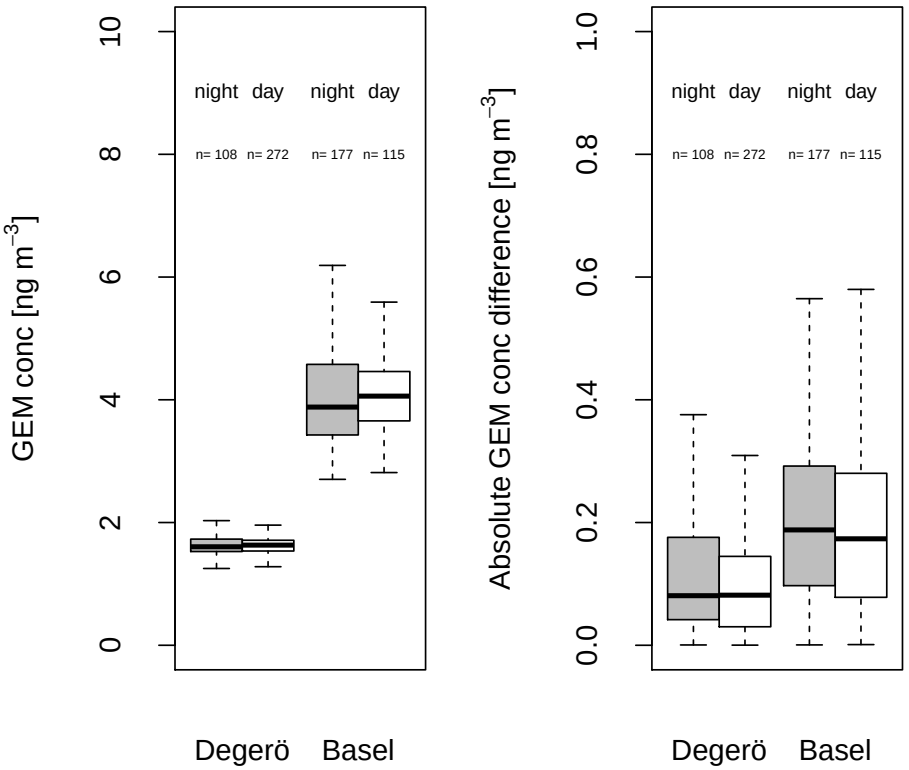

Figure 9. GEM concentration during the day and night at Degerö and Basel **(a)** and the absolute GEM concentration difference between updraft and downdraft **(b)**. Number of observations is indicated. The boxes contain interquartile range. The edges of the boxes indicates the 75th the 25th percentiles respectively. The whiskers indicate 1.5 times the interquartile range.

AMTD
8, 8113–8156, 2015

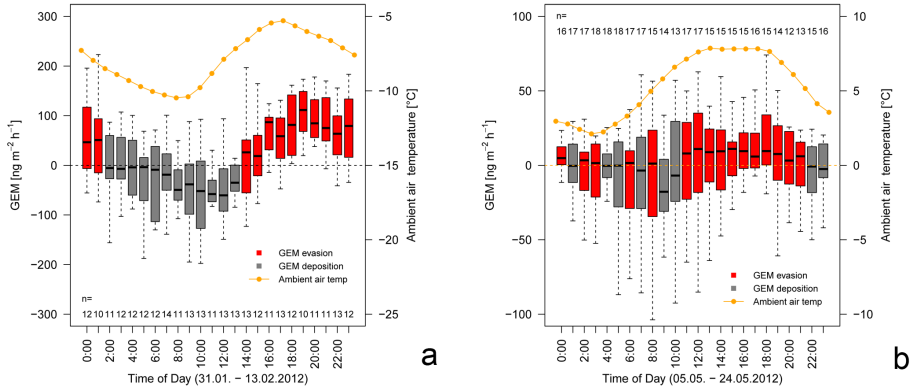

Figure 10. Diurnal patterns of GEM flux during the campaign in Basel **(a)** and Degerö **(b)** using the 6 hourly smoothed Hg flux time series. Red and gray colored boxplots indicate median Hg emission and Hg deposition at different times of the day, respectively. Average ambient air temperatures measured at height of REA inlets are given (orange). Horizontal dashed line indicates the zero line of GEM flux and/or ambient air temperature. Boxplot description in caption of Fig. 9.

AMTD
8, 8113–8156, 2015